ADVANCED MATERIALS INTERFACES
Open Access
www.advmatinterfaces.de

Surface Grafted *N*-Oxides have Low-Fouling and Antibacterial Properties

*Nils Burmeister, Eilika Zorn, Aneeq Farooq, Lena Preuss, Christel Vollstedt, Timo Friedrich, Tomi Mantel, Nico Scharnagl, Marcus Rohnke, Mathias Ernst, Sebastian G. Wicha, Wolfgang R. Streit, and Wolfgang Maison**

Low-fouling materials are often generated by surface zwitterionization with polymers. In this context, poly-*N*-oxides have recently attracted considerable attention as biomimetic stealth coatings with low protein adsorption. Herein, this study reports that poly-*N*-oxides can be grafted from plasma-activated plastic base materials. The resulting hydrophilic surfaces have low-fouling properties in bacterial suspensions and suppress the formation of biofilms. Moreover, efficient antibacterial activity against Gram-negative and Gram-positive bacteria caused by release of reactive oxygen species is observed. The latter effect is specific for polymeric *N*-oxides and is most likely triggered by a reductive activation of the *N*-oxide functionality in the presence of bacteria. In contrast to other zwitterionic polymers, *N*-oxides combine thus low-fouling (stealth) properties with antibacterial activity. The bioactive *N*-oxide groups can be regenerated after use by common oxidative disinfectants. Poly-*N*-oxides are thus attractive antibacterial coatings for many base materials with a unique combined mechanism of action.

1. Introduction

Almost all materials are rapidly covered by biomolecules and microorganisms when exposed to biological media. This so-called biofilm formation is of fundamental importance in nature and has implications for many industrial processes and the health sector.[1] For in vivo applications, the adhesion of biomolecules to surfaces contributes to immunogenicity and low blood compatibility.[2] Microbial biofilms enhance the development of resistance and increased pathogenicity of microbes[3] causing unwanted spread and/or infections in hospitals, implants, food packaging, the distribution of drinking water and other areas.[4] Low-fouling (also antifouling or stealth) surfaces are designed to prevent the attachment of biomolecules and microorganisms.[5] Low-fouling surface properties come typically with good biocompatibility of materials. This allows in vivo applications without platelet activation or the initiation of the foreign body recognition system.[6] Biocompatibility is thus often linked to low-fouling, although the two concepts are not synonymous. However, there is a strong overlap in the technology used to implement them. Surface zwitterionization, often achieved by grafting polymeric zwitterions, is a particularly successful method in this context.[7] The resulting polymer layers are strongly hydrated and they install a protective water layer at the material/solution interface.[8] Zwitterions fit therefore the requirements defined by Whitesides for low-fouling applications.[9]

Three major classes of zwitterions have been used frequently for low-fouling applications: phosphobetaines $-OPO_3^-(CH_2)_nN^+Me_3$,[10] carboxybetaines $-N^+(CH_2)_nCO_2^-$[11] and sulfobetaines $-N^+(CH_2)_nSO_3^-$.[12] It has been demonstrated that the hydration properties of these polymers depend on the alkyl spacer $-(CH_2)_n-$ between the anionic (acidic) and the

N. Burmeister, E. Zorn, A. Farooq, T. Friedrich, S. G. Wicha, W. Maison
Department of Chemistry
Universität Hamburg
Bundesstrasse 45, 20146 Hamburg, Germany
E-mail: wolfgang.maison@uni-hamburg.de

The ORCID identification number(s) for the author(s) of this article can be found under https://doi.org/10.1002/admi.202300505

DOI: 10.1002/admi.202300505

L. Preuss, C. Vollstedt, W. R. Streit
Department of Microbiology and Biotechnology
Universität Hamburg
Ohnhorststrasse 18, 22609 Hamburg, Germany

T. Mantel, M. Ernst
Institute of Water Resources and Water Supply
Technische Universität Hamburg
Denickestraße 17, 21073 Hamburg, Germany

N. Scharnagl
Institute of Surface Science
Helmholtz-Zentrum Hereon GmbH
Max-Planck-Strasse 1, 21502 Geesthacht, Germany

M. Rohnke
Institute of Physical Chemistry and Center for Materials Research
Justus-Liebig-University Giessen
Heinrich-Buff-Ring 17, 35392 Giessen, Germany

cationic ammonium group (other cations besides ammonium groups have also been used but are less common). A short alkyl spacer was found to be advantageous for optimal low-fouling properties in most studies.[13] Recently, Jiang et al. introduced consequently polymeric *N*-oxides –N^+—O^- as low-fouling and biocompatible polymers.[14] With only one sigma bond, *N*-oxides contain the smallest possible spacer to separate the charges in a zwitterion. In addition, *N*-oxides have several desirable properties for low-fouling applications. They are easy to prepare by oxidation of tertiary amines[15] and they have a dative N^+–O^- bond with extremely high charge separation compared to homologue P^+–O^- or S^+–O^- bonds. Consequently, *N*-oxides have high dipole moments of 4-5 D[16] and form strong hydrogen bonds with water.[17] This makes *N*-oxides powerful kosmotropes,[18] a property used technically, for example as kinetic hydrate inhibitors to avoid the formation of gas clathrates in gas or oil production.[19] The same properties are also used in nature for example with trimethylammoniumoxide (TMAO), a natural *N*-oxide found in seawater fish (and also in humans).[20,21] TMAO stabilizes proteins by counteracting protein-denaturing compounds (eg. chaotropes like urea) or denaturing forces like heat and pressure. It is also notable that *N*-oxides of alkaloids are non-toxic derivatives of their toxic membrane-permeable parent amines used for vesicle storage in plants and insects.[22] With the transfer of these properties to a polymeric *N*-oxide (PTMAO), Jiang et al. demonstrated that zwitterionization of surfaces with PTMAO leads to extremely low levels of blood protein adsorption and reduced fibroblast adhesion. It was also shown that protein conjugates of PTMAO were invisible to immune recognition in mice. These interesting findings trigger the question: Are polymeric *N*-oxides also efficient low-fouling reagents to prevent the formation of microbial biofilms on surfaces? Several other questions come to mind, when considering the fundamental differences of *N*-oxides compared to other zwitterions. In addition to the (favorable) properties mentioned above, *N*-oxides contain a weak N—O bond and are chemically reactive compounds.[23] This is reflected by their common use as oxidants and intermediates in organic synthesis[24] as well as biosynthesis.[25] Several *N*-oxides of low molecular weight are biologically active and have been explored as drugs.[22c,26] Reductive metabolism by microorganisms or in hypoxic tissue triggers their biological activity as antibiotics or cytotoxic compounds for chemotherapy.[27] Polymeric *N*-oxides are used as oxidants in organic synthesis,[24c] as cathode interlayer materials in organic solar cells[28] and have been found to be active against silicosis.[29] The chemical reactivity as well as the antibacterial and cytotoxic properties of many *N*-oxides raises questions about additional biological activities of polymeric *N*-oxides beyond their stealth properties.[30]

The most important questions addressed by this study are thus: 1. Do polymeric *N*-oxides on surfaces have antifouling properties for microorganisms? 2. How durable are their effects given their relatively high chemical reactivity? 3. Do polymeric *N*-oxides have other biological effects besides their stealth properties? 4. Are the biological effects of polymeric *N*-oxides different from those of their small molecule analogues? In this report, we use grafted polymeric *N*-oxides on polyethylene (PE) as a base material to address the questions above.

2. Results

2.1. Surface Grafting of Poly-*N*-Oxides to Polyethylene

Covalent zwitterionization of PE with polymeric *N*-Oxides was performed via a three-step procedure (**Figure 1**). Briefly, the chemically unreactive PE surface was activated through an atmospheric plasma treatment. The resulting reactive functionalities serve as anchor points for heat-induced graft polymerization of a suitable precursor of the methacrylate- or vinylbenzyl-type (either VBDMA, MADMA or MAADMA) to form the corresponding polymer brushes (poly-VBDMA, poly-MADMA or poly-MAADMA). These two initial steps followed an established procedure for surface modification of PE from our lab.[31] Final zwitterionization of the polymer brushes was achieved by post-grafting oxidation with H_2O_2. An alternative direct polymerization of monomeric *N*-oxides of the methacrylate- or vinylbenzyl-type (as described for the syntheses of other polymeric *N*-oxides)[14] was not an option here because the *N*-oxide moieties were found to be not compatible with the heat-induced polymerization protocol employed. Successful grafting and subsequent oxidation were reflected by extremely low static contact angles $\theta = 10–30°$ with water for the resulting materials PE-poly-(VBNOx), PE-poly-(MAANOx) an PE-poly-(MANOx) (**Table 1**). In addition, the presence of poly-*N*-oxides was confirmed by combined 3D mass spectrometric and scanning probe microscopy (SPM) analysis by a variety of characteristic nitrogen and oxygen-containing organic mass fragments such as CN^- and CNO^- (**Figure 2**). SPM images taken before and after depth profiling with a time-of-flight secondary ion mass spectrometer (ToF-SIMS) revealed a surface roughness R_a of 1–2.5 µm and a brushlayer thickness of ≈50–100 nm.

The successful immobilization of polymeric *N*-oxides on PE was also verified by ATR-FTIR spectroscopy and X-ray photoelectron spectroscopy (XPS) analysis. Exemplary data is depicted in **Figure 3** (see Figure S1, Supporting Information for IR-spectra of other materials). The FTIR-spectra of PE-poly-(VBNOx) in Figure 3a reveal the characteristic N-O vibration at 933 cm^{-1}, which is also visible in the monomer (VBNOx) spectrum. These characteristic N—O bands are also observed for the other zwitterionic materials PE-poly-(MANOx) and PE-poly-(MAANOx), along with carbonyl bands from the polymethacrylate and polymethacrylamide backbones (spectra not shown, see Figure S1, Supporting Information). For full characterization of the grafting process, we performed XPS measurements of pristine PE, plasma activated PE and modified poly-(*N*-oxide)-PE (see SI for additional spectra). The spectra revealed the presence of peroxides on the PE surface after plasma activation with a dominant peak at 532.4 eV in the O1s spectra (Figures S3 and S4, Supporting Information). The atomic ratios of N/C was 0.07 which is similar to the theoretical value of 0.09 and indicates successful radical polymerization and subsequent oxidation to PE-poly-(VBNOx) (Figure S5, Supporting Information). Slight deviation of the theoretical atomic ratios of N/O and O/C can be explained by impurities, probably associated to polymer entrapped carbon monoxide and/or water. The deconvoluted peak at 402.6 eV in the N1s spectra was assigned to the quaternary ammonium group in the N—O bond which is also reflected by a peak at 531.0 eV in the O1s spectra (Figure 3b). Both, N1s and

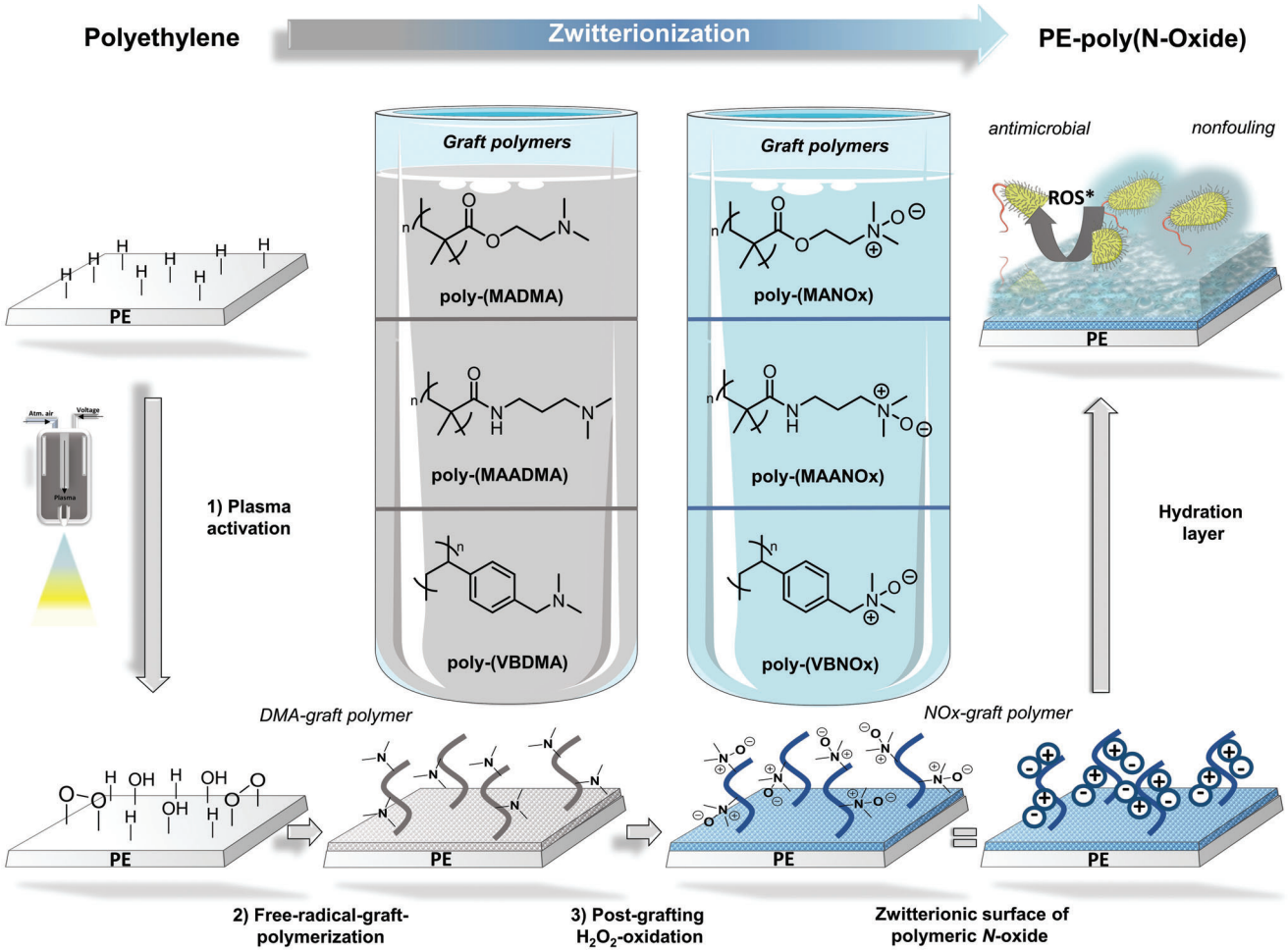

Figure 1. Surface grafting of *N*-oxides to PE foils. 1) Plasma activation of otherwise inert PE, 2) heat-induced radical polymerization, 3) post-grafting zwitterionization of the polymer brushes by oxidation of tertiary amines to *N*-oxides with H_2O_2.

O1s binding energies are consistent with previous reports on polymeric *N*-oxides. N1s spectra indicate good conversion of tertiary amines to the corresponding *N*-oxides by H_2O_2-treatment for 72 h. However, the signal at 399.3 eV can be assigned to residual tertiary amines. Furthermore, a detailed deconvolution of N1s spectra reveals an additional small signal at 400.3 eV, which is also detectable in the survey spectra of pristine PE (Figures S2,S5, and S6, Supporting Information). These minor impurifications are due to non-identified nitrogen species on the surface.

2.2. Microbiological Assessment of Low-Fouling Activity

The low-fouling activity of PE with three different grafted *N*-oxides was tested with a bacterial adhesion assay and a LIVE/DEAD staining.[31b,32] *Staphylococcus aureus* (Gram-positive, strain ATCC29213) was used as a model pathogen. It is a clinically relevant pathogen responsible for many health care related infections.[33] In addition, *Vibrio campbellii* (previously classified as *Vibrio harveyi*) (Gram-negative, strain BB120 was used as a second model organism because it is a major

Table 1. Polymerization conditions and water contact angles (WCA) for grafted polymers on PE.

Entry	Monomer [wt%]	AIBN [wt%]	PE-poly-(XXDMA), WCA [°] [a]	PE-poly-(XXNOx), WCA [°] [a]
1	–	–	–	pristine PE, 95.2 ± 1.6
2	VBDMA, 40	1.0	PE-poly-(VBDMA), 9.9 ± 1.4	PE-poly-(VBNOx), 9.9 ± 1.4
3	MADMA, 20	0.1	PE-poly-(MADMA), 19.8 ± 2.	PE-poly-(MANOx), 19.8 ± 2.3
4	MAADMA, 40	0.1	PE-poly-(MAADMA) 29.4 ± 1.9	PE-poly-(MAANOx) 29.4 ± 1.9

[a] Advancing WCA were measured with deionized water using the static sessile drop method and are given as mean value ± SD of at least three independent samples.

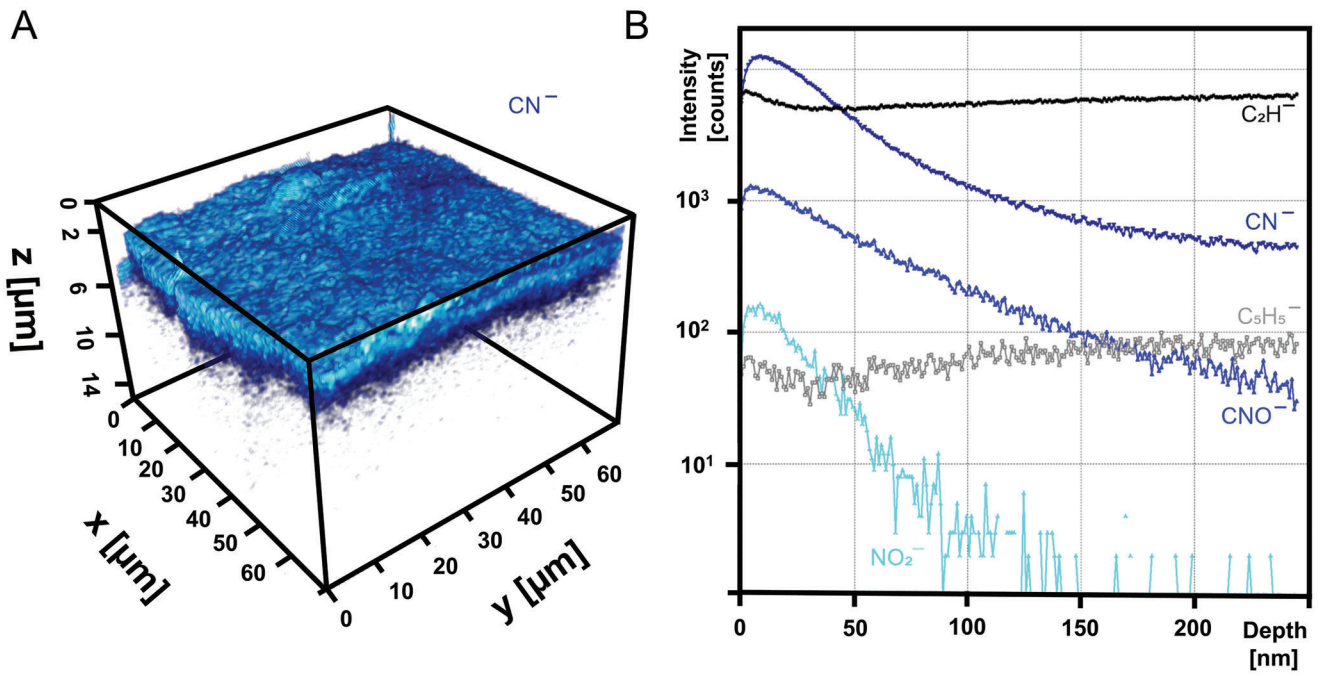

Figure 2. Combined 3D ToF-SIMS and SPM imaging analysis of PE-poly-(VBNOx). A) Correlative SPM/SIMS-3D image of the poly-(VBNOx) coating layer with the spatial distribution of CN^- as the most intensive ion on top of the substrate. Shades of blue correspond to signal intensity of CN^-. B) ToF-SIMS depth profile of PE-poly-(VBNOx) with poly-(VBNOx)-specific nitrogen containing mass fragments CN^-, CNO^-, and NO_2^- and characteristic PE fragments C_2H^- and $C_5H_5^-$. SIMS analysis was performed in negative ion mode with Bi_3^{++} ions. Depth profiling was carried out using Ar^+_{2000} cluster ions for sputtering.

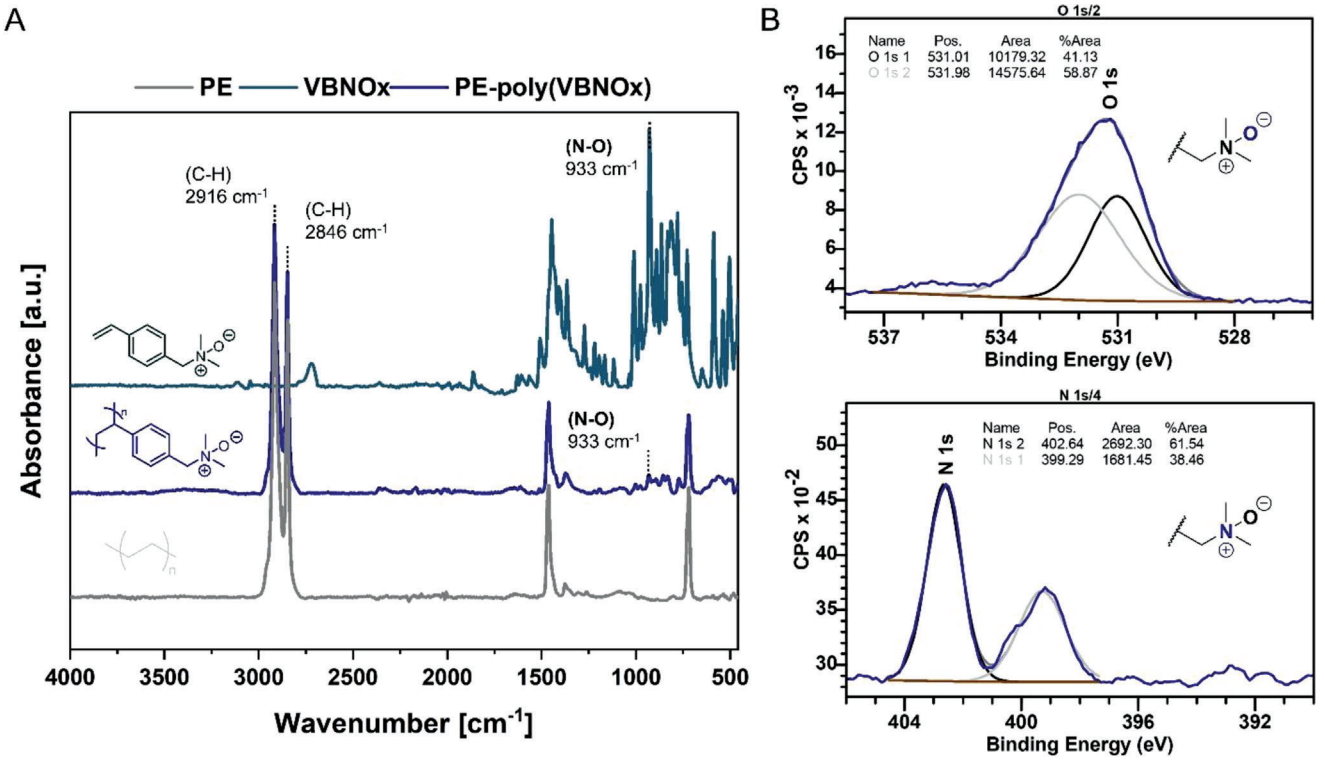

Figure 3. Characterization of PE-poly-(VBNOx) by ATR-FTIR and XPS. A) ATR-FTIR spectra in absorbance mode of pristine PE, PE-poly-(VBNOx), and VBNOx monomer for comparison. B) Deconvoluted regions of O1s and N1s XPS spectra of PE-poly-(VBNOx). Survey spectra of pristine PE, plasma activated PE and PE-poly-(VBNOx) are available in the supporting material.

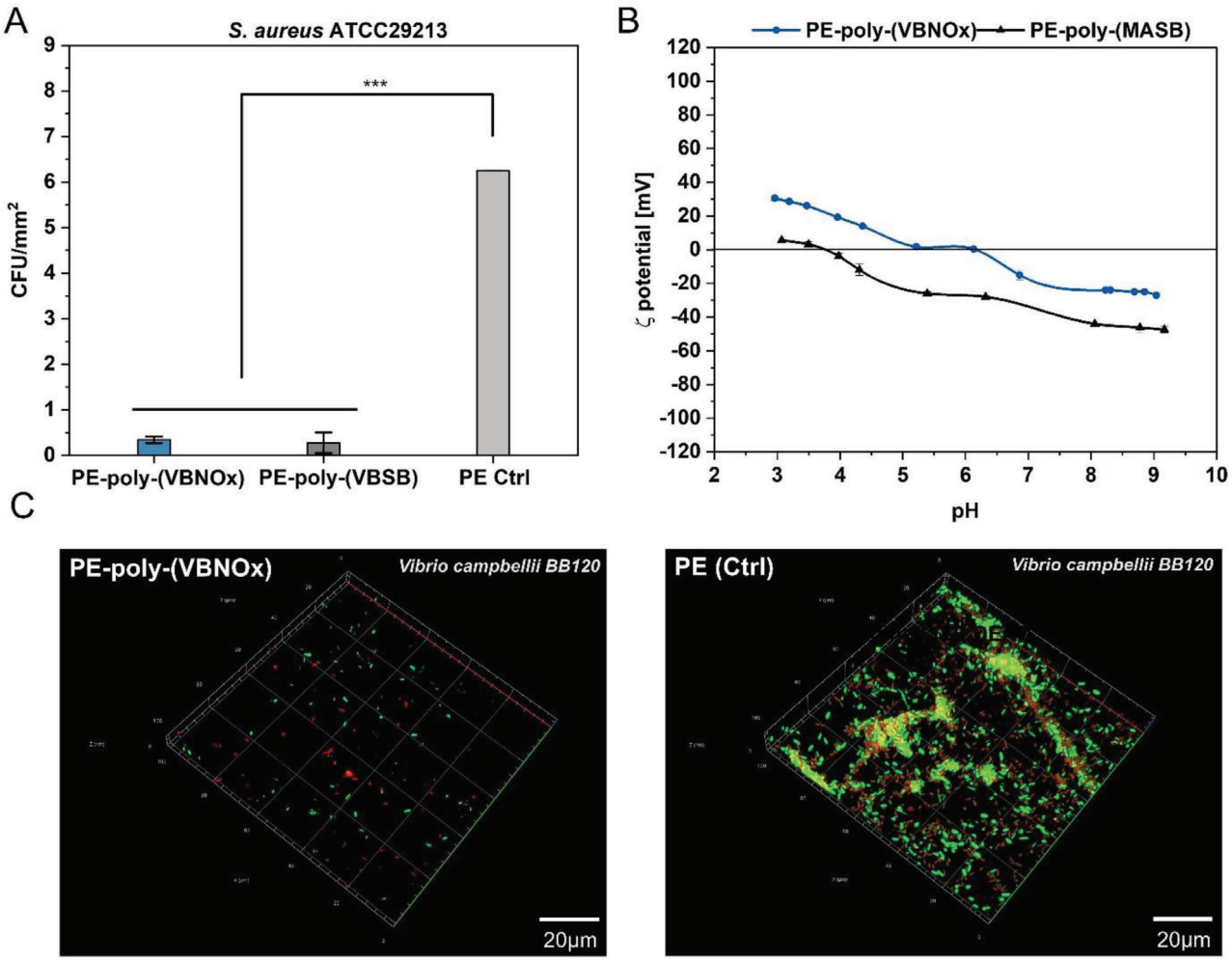

Figure 4. Microbiological assessment of low-fouling surfaces. A) Bacterial adhesion assay with *S. aureus* (strain ATCC29213): Colony counts after incubation of PE-poly-(VBNOx), PE-poly-(VBSB) and pristine PE as control (Ctrl) with *S. aureus* (initial concentration: 10^5 CFU mL^{-1} in MHB) for 24 h. Statistical significance was determined via pairwise comparison (Tukey test) $p \leq 0.001$ (***). B) Zeta potential measurement of PE-poly-(VBNOx) and PE-poly-(MASB) at pH 3–9. C) Biofilm adhesion: confocal microscopy of PE-poly-(VBNOx) (left) and PE (right) after 24 h incubation with *V. campbellii* (strain BB120) in artificial seawater, followed by LIVE/DEAD™ staining. Live bacteria appear light green, dead bacteria red. The images indicate representative areas within static biofilms.

contributor to the marine microbiome and has also been identified as a potential pathogen in coastal water. Moreover, *V. campbellii* forms rapidly biofilms on plastic substrates (particularly on PE) accompanied with high antibiotic resistance.[34] Briefly, sterilized test specimens (size: 1.0 cm^2) were fully immersed in a bacterial suspension (10^2–10^5 CFU mL^{-1}) and stored with gentle shaking ensuring complete contact of the materials with the inoculum. After 24 h, samples were transferred into a sterile saline solution to desorb loosely attached microbes. Growth controls of each media were collected at this point to verify presence and concentration of living bacteria. Finally, test specimens were printed carefully onto an agar plate (Columbia Agar) and were subsequently incubated at 37 °C for 20 h before colony counting. Pristine PE specimens were used as controls. In addition, a poly-sulfobetaine grafted zwitterionic PE sample (PE-poly-(VBSB)) with known excellent low-fouling properties was used for comparison.[31b] The results shown in **Figure 4**a reveal a low-fouling effect of the grafted polymeric *N*-oxide on PE (PE-poly-(VBNOx)), comparable to the corresponding polymeric sulfobetaine control material (PE-poly-(VBSB)). A second adhesion assay was performed with the marine organism *V. campbellii* in artificial seawater, followed by confocal microscopy after a LIVE/DEAD staining (LIVE/-DEAD BacLight Viability Kit). The resulting images after incubation confirmed the low-fouling activity of PE-poly-(VBNOx) and show almost no adhering live bacteria (green fluorescence) on PE-poly-(VBNOx) after 24 h immersion in seawater whereas pristine PE was rapidly colonized by bacteria (Figure 4C). Polymeric *N*-oxides like poly-(VBNOx) have thus excellent low-fouling activity against the here tested Gram-negative and Gram-positive bacteria and are competitive with established zwitterionic materials such as polysulfobetaines. *N*-oxides (pKa ≈4–5) have significantly higher pKa values than sulfonic acids in sulfobetaines (pKa ≈1–2). The zeta potential of zwitterionic materials bearing sulfobetaines is thus strongly negative in a broad pH range.[35] In contrast, the analysis of poly-*N*-oxide materials like PE-poly-(VBNOx) revealed

only slightly negative to neutral zeta potentials at biologically most relevant pH values of 5–8.[36] Neutral surface zeta potentials were previously found to be ideal for optimal low-fouling performance.[35]

2.3. Antibacterial Activity of Poly-(*N*-Oxides)

The observed low-fouling activity of polymeric *N*-oxides against bacteria has not been described before. However, it is not surprising, given the reported low protein fouling of these materials.[14,36] It was notable though, that a dramatic antimicrobial effect was observed in the growth controls of the adhesion assays. When bacterial solutions were exposed to PE-poly-(VBNOx) almost all bacteria were immediately killed. This was a striking contrast to growth controls of pristine PE and also sulfobetaine PE-poly-(VBSB). Both did not reveal any antibacterial effect. The antimicrobial activity of three different *N*-oxides was therefore confirmed by a quantitative analysis according to ASTM E2149-13a, a common assay to evaluate antimicrobial materials.[37] We selected *S. aureus* (Gram-positive, strain ATCC29213) and *E. coli* (Gram-negative, strain ATCC25922) for the assay. Briefly, sterilized PE test specimens were immersed with bacterial solutions of 10^5 CFU mL^{-1} at 37 °C. After incubation for 2 h, the resulting solutions were aliquoted in *log* levels ranging from 10^5–10^2 CFU mL^{-1} onto Columbia agar and were subsequently incubated for 17 h before colony counting. Results are depicted in **Figure 5** and reveal a remarkable antimicrobial effect of the poly-*N*-oxide-grafted materials for both Gram-positive *S. aureus* and Gram-negative *E. coli*.

The antimicrobial effect was confirmed for all three polymeric *N*-oxides tested and is thus not dependent of the polymer backbone structure. However, the methacrylamide-derivative PE-poly-(MAANOx) showed a lower antimicrobial effect than both other *N*-oxides. This might indicate an effect of the alkyl-spacer length or the linking functionality (amide vs ester) of the polymerizable group on antibacterial activity. Either a release of antimicrobial compounds from the material or a contact-active mechanism might explain the observed antibacterial effect. The latter would be principally possible due to the high pK_a value of *N*-oxides. This might cause protonation under slightly acidic conditions created by colonizing bacteria. Significant protonation of PE-poly-(VBNOx) starts at pH values lower than 4, leaving a positively charged and thus possibly contact-active surface, as evident from the zeta potential measurements in Figure 4B. However, such low pH values have only been reported locally in biofilms.[38] We have not detected any biofilm formation or adhesion of bacteria to the *N*-oxide test specimens in our adhesion assays making contact activity unlikely. Further evidence for a release mechanism came from an agar plate diffusion test (DIN EN ISO 20645:2002-02) with *S. aureus* and *E. coli*. An inhibition zone around the poly-*N*-oxide test specimen was clearly visible supporting leaching of antimicrobial compounds (Figure S7, Supporting Information). Release of residual H_2O_2 from the oxidative preparation of *N*-oxide polymer brushes was excluded through inspection of the XPS spectra and via a horseradish peroxidase assay (Figure S10, Supporting Information)[39] This assay is sensitive to H_2O_2-concentrations in the micromolar range which is orders of magnitudes lower than the MIC of H_2O_2 for *S. aureus* (MIC = 0.27-0.66 mM) and *E. coli* (MIC = 1.33-2.66 mM).[40]

As mentioned in the introduction, some *N*-oxides have been reported to have antimicrobial or cytotoxic properties. These compounds are typically benzotriazine dioxides or phenazine dioxides of low molecular weight. A prototype is tirapazamine (TPZ, MW = 178 g mol^{-1}), an experimental anticancer drug and antibiotic. The mode of action of TPZ involves most likely a reductive activation leading to the formation of cytotoxic hydroxyl radicals by cleavage of a N—O bond.[27] The latter homolytic bond cleavage is not surprising because the bond dissociation energies of *N*-oxides are known to be relatively low.[23] However, the formation of reactive oxygen species from *N*-oxides under physiological conditions has been reported for a limited set of compounds only but not for polymeric *N*-oxides.[27] The formation of radical species from grafted polymeric *N*-oxides was tested with DPPH*, a stable radical commonly used as a radical scavenger. The DPPH*-radical has an absorption maximum at 520 nm and the loss of absorption intensity at this wavelength can be correlated to the formation of radical adducts.[41] Treatment of PE-poly-(VBNOx) with DPPH* at 37 °C lead to significant scavenging of DPPH* after 2 h and almost complete DPPH* consumption after 24 h (**Figure 6**a). In contrast, the corresponding monomeric *N*-oxide VBNOx leads to only minor consumption of DPPH* after 24 h suggesting that only polymeric *N*-oxides generate potentially antibacterial radical species under physiological conditions. The identity of the generated radicals was analyzed by electron paramagnetic resonance (EPR)-spectroscopy after treatment of PE-poly-(VBNOx) with DMPO as a spin trap. The resulting EPR spectra show the presence of a radical trapped by DMPO (Figure 6b). The analysis of respective hyperfine coupling constants (a_N = 15.9 G and a^{β}_{H} = 4.1 G) revealed an oxygen-centered radical, either a hydroxyl-radical (OH*) or a superoxide-radical (O^{2-}*)[42] and is a clear indication of released reactive oxygen species (ROS-formation). Again, generation of ROS species was found to be specific for the grafted polymeric *N*-oxides but was not observed for the monomeric *N*-oxide (VBNOx) (Figure 6). In consequence, no antibacterial activity of VBNOx was detected and we determined minimal inhibitory concentrations (MIC) of VBNOx > 1024 μg mL^{-1} for *E. coli* and *S. aureus* (Table S1, Supporting Information).

The release of ROS from polymeric *N*-oxides triggered questions regarding the fate of the material and the durability of the observed antibacterial effect. Specimens of PE-poly-(VBNOx) were therefore repeatedly exposed to bacteria according to ASTM E2149-13a. **Figure 7** shows the results of these experiments. They reveal a retained activity of the material after repeated use with no measurable loss in function. The antibacterial activity after repeated use is not dependent on intermediate purification and treatment of the test specimens before the next incubation experiment. Intermediate treatment of PE-poly-(VBNOx) with three different disinfection reagents (NaOCl, H_2O_2 and *i*PrOH/PrOH/EtOH (BacillolAF)) lead to identical antibacterial activity of the material. Activity is also retained if no disinfection is performed between incubations. However, the transfer of residual bacteria leads to a significantly higher (>10^5 CFU mL^{-1}) initial concentration of bacteria in the test solutions after repeated incubation. The resulting high inoculum leads to a slight

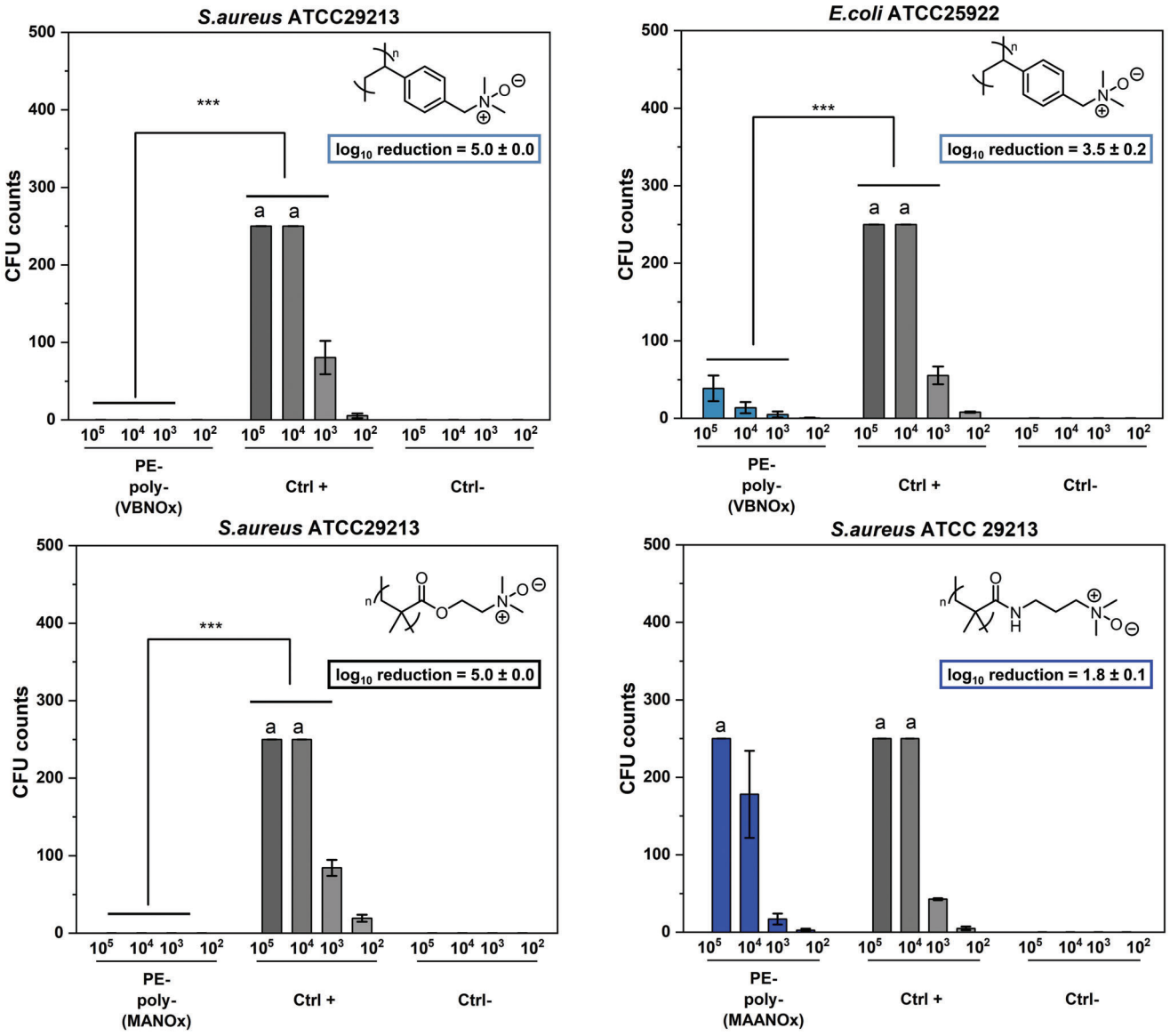

Figure 5. Antibacterial activity of three different grafted polymeric *N*-oxides on PE measured by ASTM E2149-13a. Colony counts after incubation of PE test specimens with bacterial suspensions at different dilutions (10^5–10^2 CFU mL^{-1}) for 2 h. Each experiment was performed in triplicate, pristine PE (Ctrl +) and pure saline (Ctrl -) were used in control experiments. Colony counts above 250 were set as "too numerous to count" (TNTC) (a). Log10 reduction was calculated as described in the experimental. Statistical significance was determined via pairwise comparison (Tukey test) $p \leq 0.001$ (***), $p \leq 0.01$ (**).

increase of surviving bacteria after the repeated 2 h exposure to the PE-poly-(VBNOx) specimen. Analysis of the test specimens after repeated exposure to microorganisms revealed identical chemical and physical properties of the material. It is notable that we observed no degradation of the grafted polymeric *N*-oxides. Chemical degradation processes of *N*-oxides can lead to the formation of hydroxylamines and carbonyl groups, although these conversions are typically observed at higher temperatures than our test conditions.[15,24a] We did not find any evidence for these functional groups and in addition, the contact angle and the zeta potential of the materials remained constant after threefold use (Figure S13, Supporting Information). The release of ROS from polymeric *N*-oxides at room temperature is most likely a consequence of a reductive activation of the *N*-oxide in the presence of microorganisms. It might thus follow the same mechanisms reported for cytotoxic activation of some *N*-oxides in hypoxic tumor tissue.[26a,b,27,43]

3. Discussion

Three different polymeric *N*-oxides were successfully grafted to PE as a base material. We have used an established two-step protocol involving atmospheric plasma activation of PE and subsequent heat-induced graft polymerization of methacrylate,

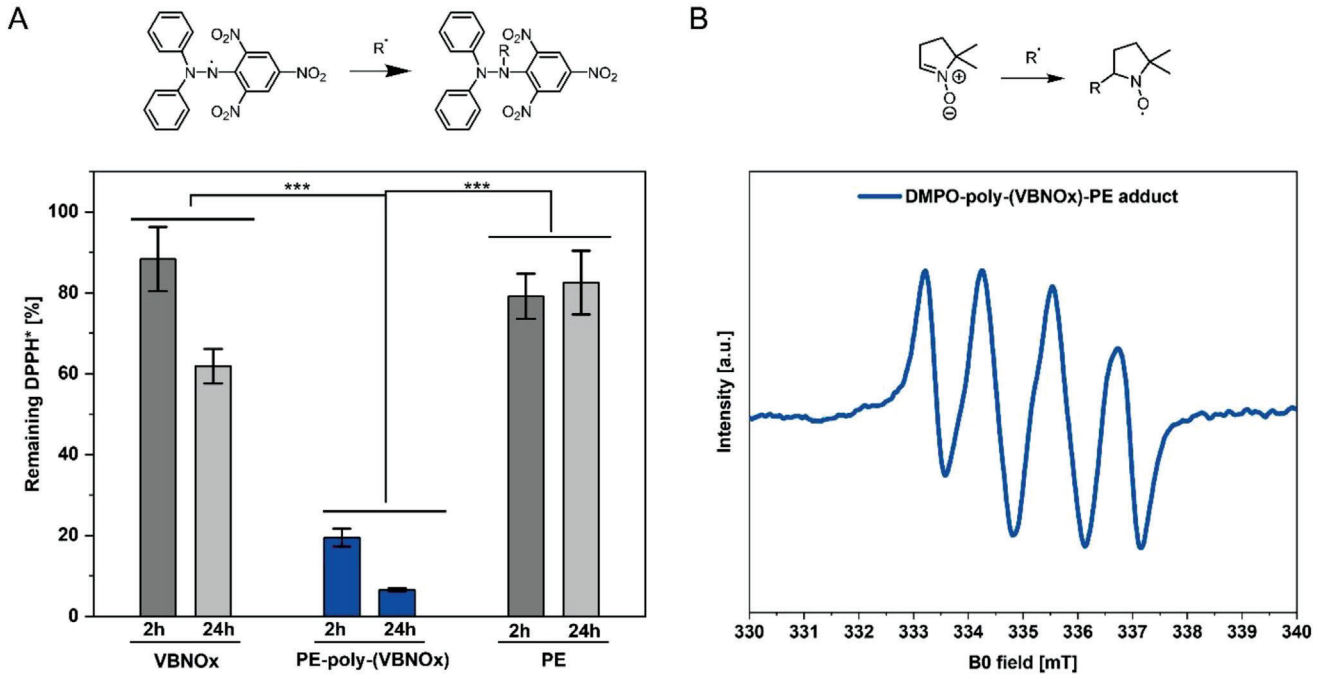

Figure 6. Evaluation of ROS formation from PE-poly-(VBNOx). A) DPPH radical scavenging and remaining DPPH-radical after exposure to VBNOx (1024 µg mL^{-1}), PE-poly-(VBNOx) (surface area: 1 cm^2), and pristine PE (surface area: 1 cm^2) at 37 °C in MeOH. B) EPR spectra after treatment of DMPO with a PE-poly-(VBNOx) specimen (surface area: 1 cm^2). Control experiments were performed with pristine PE + DMPO and PE-poly-(VBNOx) without DMPO, data available in the supplementary material (Figure S12, Supporting Information). Statistical significance was determined via pairwise comparison (Tukey test) $p \leq 0.001$ (***).

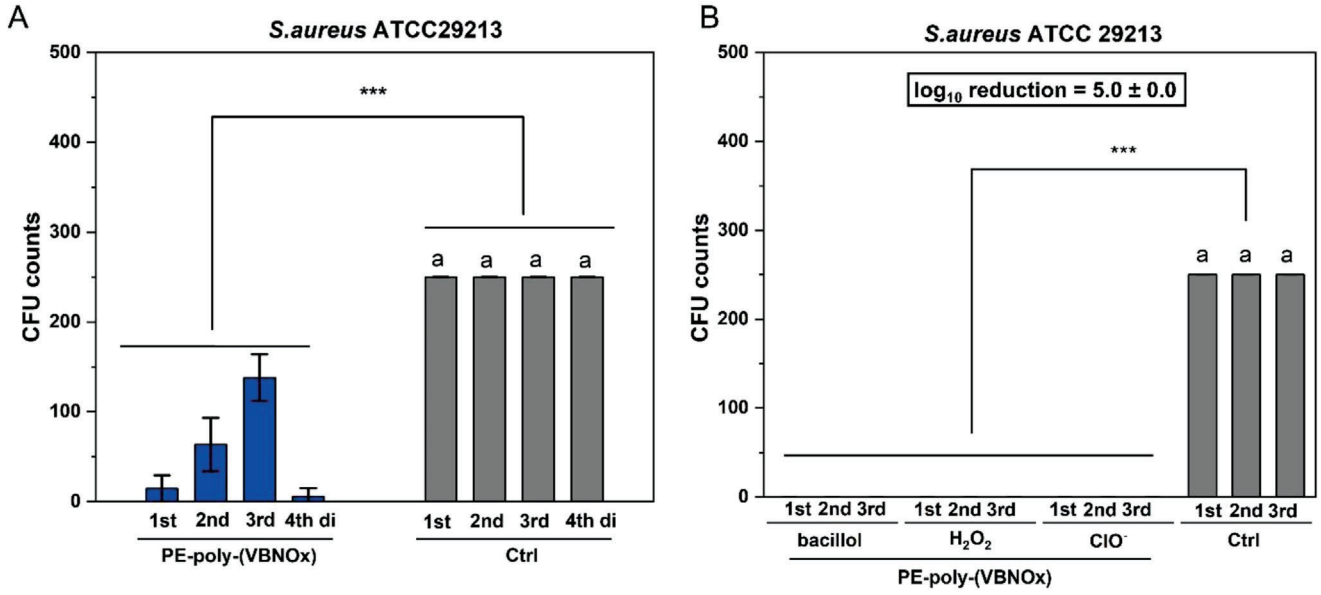

Figure 7. A) Repeated use of pristine PE (Ctrl) and PE-poly-(VBNOx) specimens (surface area: each 1.0 cm^2) in an antibacterial assay following ASTM E2149-13a. The test specimens were exposed to the incubation solutions without intermediate disinfection three times (1st, 2nd, 3rd). An additional fourth exposure was performed after H_2O_2 disinfection (4th di). B) Repeated antibacterial assay (ASTM E2149-13a with *S. aureus*) for pristine PE and PE-poly-(VBNOx) specimens (surface area: each 1.0 cm^2). The test specimens were exposed to new incubation solutions (10^5 CFU mL^{-1}) after intermediate disinfection (BacillolAF: *i*PrOH/PrOH/EtOH, aqueous H_2O_2 (30% v/v) and aqueous NaOCl (12% v/v)) three times (1st, 2nd, 3rd). Bars represent mean values ± SD of three independent measurements. Colony counts above 250 were set as "too numerous to count" (TNTC) (a). Statistical significance was determined via pairwise comparison (Tukey test) $p \leq 0.001$ (***).

methacrylamide and vinylbenzene monomers. The process generates covalently linked dense polymer brushes of polymeric tertiary amines. These were oxidized with H_2O_2 to the target polymeric *N*-oxides in a final step. The resulting materials were characterized by IR, XPS and ToF-SIMS confirming the complete conversion of tertiary amine groups to the corresponding *N*-oxides. We found a brush layer thickness of ≈50–100 nm for the grafted polymeric *N*-oxides. The surfaces are characterized by extremely low static contact angles $\theta = 10–30°$ with water and almost neutral zeta potentials in the pH range from 5–7 for PE-poly-(VBNOx), PE-poly-(MAANOx) and PE-poly-(MANOx). The latter parameter distinguishes grafted poly-*N*-oxides from other poly-zwitterions such as sulfobetaines which have negative zeta potentials at pH values as low as 4, reflecting the higher acidity of sulfonic acids (pk_a ≈1–2) compared to *N*-oxides (pk_a ≈4–5).

The whole process of *N*-oxide grafting described herein is scalable and uses readily available starting materials. It should also be applicable to many other plastics besides PE as a base material. However, the heat-induced graft polymerization is not compatible with monomers containing *N*-oxides because these are intrinsically unstable at higher temperatures. This is a notable difference to other grafting procedures such as copper catalyzed surface-initiated atom transfer radical polymerization (SI-ATRP), which has been shown to be compatible with *N*-oxide monomers.[14] The low water contact angles and the almost neutral zeta potentials of all three grafted poly-*N*-oxides (PE-poly-(VBNOx), PE-poly-(MAANOx) an PE-poly-(MANOx)) are ideal parameters for low-fouling surfaces. These stealth properties of poly-*N*-oxides have been shown to prevent protein adhesion before.[14,36,44] It was therefore not surprising that we also observed good low-fouling properties in bacterial adhesion tests against *S. aureus*, an important pathogen for health care related infections and *V. campbellii*, a marine microorganism.

However, beside the confirmation of a low-fouling effect for poly-*N*-oxides, the growth controls of these adhesion experiments revealed clear antibacterial properties. These were confirmed in standard ASTM assays with Gram-negative and Gram-positive bacteria. We attribute these antibacterial properties to the generation and release of radicals, which we confirmed at 37 °C via DPPH as a radical scavenger. The resulting EPR spectra of DMPO-radical adducts revealed the generation of ROS from poly-*N*-oxide surfaces. Other possible reasons for the antibacterial properties of poly-*N*-oxides such as contact-activity through protonation of *N*-oxides or release of residual (antibacterial) H_2O_2 are unlikely. A release mechanism is clearly supported by an inhibition zone around the PE-poly-*N*-oxide specimens which would not be observed for a contact-active material. Release of residual H_2O_2 was excluded via a sensitive HRP-assay. The generation of ROS from *N*-oxides under physiological conditions has been reported for a limited set of aromatic *N*-oxides of low molecular weight only. It has been reported that the release of ROS from drugs containing *N*-oxide groups (e.g., tirapazamine) is triggered in hypoxic tumor tissue or in the presence of bacteria by reductive activation. In this context it is remarkable that we found the generation of ROS to be an exclusive feature of poly-*N*-oxides (PE-poly-(VBNOx), PE-poly-(MAANOx) and PE-poly-(MANOx)) and it was not observed in close analogues of low molecular weight such as VBNOx, MANOx or MAANOx. The latter compounds did not show any ROS formation and did also not have appreciable levels of antibacterial activity (MICs > 1024 μg mL^{-1} against *E. coli* and *S. aureus*).

We propose that the formation of ROS from poly-*N*-oxides follows a similar mechanism as tirapazamine and derivatives. Further evidence for this hypothesis comes from a recent report of Gao and coworkers.[43a] In this study, polymeric *N*-oxides were used as selective drug carriers for hypoxic tumor tissue (see also[45]) due to their bioreduction by CYP450-enzymes. We suspect that a similar reductive conversion of poly-*N*-oxides occurs in the presence of microorganisms leading to ROS release and thus antibacterial activity. In contrast to the most common chemical *N*-oxide degradation mechanisms mentioned above, this bioreductive pathway reduces PE-poly-(VBNOx), PE-poly-(MAANOx) an PE-poly-(MANOx) back to the corresponding polymeric tertiary amines PE-poly-(VBDMA), PE-poly-(MAADMA) and PE-poly-(MADMA). The *N*-oxides could then be regenerated from these polyamines explaining the constant antibacterial effects of polymeric *N*-oxides even after repeated exposure to bacteria. This reoxidation step might be mediated by oxidative disinfectants like NaOCl and H_2O_2. Remarkably, we noted no loss of antibacterial activity for repeated use of poly-*N*-oxides even without oxidative intermediate treatment (disinfection with BacillolAF) or even without intermediate disinfection. These latter findings might suggest self-replenishing properties of poly-*N*-oxides, presumably mediated by molecular oxygen either in solution or in air. Both the release of ROS (and thus antibacterial activity) and the reoxidation of the material are clearly special properties of the polymeric *N*-oxide because neither significant ROS production nor antibacterial activity was observed with the corresponding monomeric *N*-oxides of low molecular weight. These special properties might be caused by the close assembly of multiple *N*-oxide functionalities and thus a neighbor group effect in the polymer. Similar effects have been proposed to operate in charge transfer from polymeric *N*-oxides used in intermolecular n- or p-doping processes in optoelectronic devices.[28a,46] Neighbor group effects of polar groups have also been proposed to accelerate oxidations of tertiary amines of low molecular weight.[47]

4. Conclusion

Our studies reveal that grafted polymeric *N*-oxides are attractive low-fouling coatings for plastic base materials and might thus find application in many fields related to bacterial biofilm formation. In contrast to other zwitterionic polymers poly-*N*-oxides do not only generate stealth surfaces upon grafting but have unique antibacterial properties caused by the release of ROS. Poly-*N*-oxides combine thus low-fouling properties with the release of antibacterial compounds in a rather simple polymer. In addition, the biologically active *N*-oxide functionality can easily be regenerated upon oxidation with common disinfectants. Even without added oxidants, we noted antibacterial activity of poly-*N*-oxides upon repeated challenge of our materials with bacteria. However, whether this effect is caused by *N*-oxide regeneration or the large reservoir of *N*-oxide functionalities on the surface needs to be confirmed in future studies. The combined low-fouling and antibacterial mode of action enables applications requiring the eradication of bacteria. If ROS formation limits in vivo applications of poly-*N*-oxides needs to be determined in future studies. However, current in vivo data do not support toxic effects of poly-*N*-

oxides,[14,43a,b,45,48] which is plausible assuming that ROS release is only triggered in hypoxic tumor tissue or in the presence of bacteria.

5. Experimental Section

Chemicals and Materials: Polyethylene (LD-PE) with a thickness of 750 µm was purchased from Goodfellow and were used as received. Vinylbenzylchloride (90 %), dimethylamine solution (33 % in ethanol), azo-bis-(isobutylonitrile) (AIBN) (98 %), hydrogen-peroxide solution (30 % v/v in water), (2-dimethylaminoethyl) methacrylate (99 %), *N*-[3-diemthylamino)-propyl]-methacrylamide (99 %), 2,2-diphenyl-1-pikryl-hydrazyl (DPPH), 5,5-dimethyl-1-pyrrolin-*N*-oxide (DMPO), horseradish peroxidase (250 units per mg), pyrogallol (99 %) were purchased from Sigma-Aldrich. Microorganisms *S.aureus* (strain ATCC29213), *E.coli* (strain ATCC29522) and *Vibrio campbellii* (strain BB120 also known as strain ATCC-BAA-1116) were purchased from American Type Culture Collection. All reagents were used without further purification. Crimp neck vials (N20, 10 mL volume) and crimp caps (N20, PTFE septum) for degassing were purchased from Macherey-Nagel GmbH (Düren, Germany).

Atmospheric Air Plasma: For plasma activation, an atmospheric air plasma system from Plasmatreat GmbH (Steinhagen, Germany) was used. The atmospheric-pressure plasma was produced by a generator FG5001 with an applied working frequency of 21 kHz, generating a non-equilibrium discharge in a rotating jet nozzle RD1004 in combination with the stainless-steel tip No. 22826 for an expanded treatment width of ≈22 mm. Additionally, the jet nozzle was connected to a Janome desktop robot type 2300N for repetitious accuracy regarding treatment conditions. The process gas was dry and oil-free air at an input pressure of 5 bar in all experiments.

IR- and UV/Vis Spectroscopy: Infrared spectra were recorded with an attenuated total reflectance Fourier Transform infrared system (ATR-FTIR), model "IRAffinity-1S" from Shimadzu (Kyoto, Japan) using a "Quest" ATR accessory from Specac. The spectral range was set at 4000 cm^{-1}–400 cm^{-1} with a resolution of 0.5 cm^{-1} in absorbance mode and spectra were processed with OriginPro 9 (2021) software. UV/vis spectra were obtained on a Genesys 10S spectrophotometer from Thermo Scientific (Waltham, USA) using Visionlite software for analysis.

Contact Angle Measurements: Contact angles were acquired with an OCA 20 goniometer from DataPhysics (Filderstadt, Germany) equipped with two automated dispensing units for different liquid probes, a high-speed video system with CCD-camera, measuring stage and halogen-lighting for static and dynamic contact angle measurements. For evaluation, independent triplicate measurements at three different points of the surface were done. Advancing contact angles were measured with deionized water using the static sessile drop method with a dispensing volume of 5 µL. The dispensing rate of the automatic syringe was set at 1 µL min^{-1}. The obtained angle was calculated with the OCA software.

Electrokinetic ζ-Potential Measurements: The surface zeta potential (ζ-potential) was determined as streaming potential using an electrokinetic analyzer Surpass (Anton Paar, Graz, Austria). The measurements were carried out using an adjustable gap cell in which two samples with a rectangular size of 1 cm x 2 cm were clamped vis-á-vis with a micro slit of 110 µm in between. For each measurement, the starting conductivity was set to 17 µS m^{-1} with KCl as electrolyte. The pH was adjusted from 9.5–2.5 stepwise with automatic pH titration by adding 0.05 M HCl. Presented values of z potentials were determined as mean value of four measurements for each pH step.

Nuclear Magnetic Resonance (NMR) Spectroscopy: The measurements were performed in 5 mm o.d. sample tubes using either a Bruker Avance 600, 500, or 400 MHz (AV600, AV500 and AV400, Bruker, Ettlingen, Germany). The obtained spectra were processed with MestReNova x64 software. ^{13}C-spectra were recorded with ^{1}H-decoupling. Peak assignments were supported by 2D NMR experiments like $^{1}H,^{1}H$-COSY, $^{1}H,^{13}C$-HSQC and $^{1}H,^{13}C$-HMBC.

Time of Flight Secondary Ion Mass Spectrometry (Tof-SIMS) and Scanning Probe Microscopy (SPM): The analysis was carried out with an M6 Plus machine (IONTOF Company, Münster, Germany). Here a scanning probe microscope is included in the main vacuum chamber of the ToF-SIMS, which offers the possibility for correlation of topographic and mass spectrometric imaging data. For SIMS analysis 60 keV Bi_3^{++} primary ions were used (I = 0.05 pA at 200 µs cycle time). The Bi gun (nanoprobe 50) was operated in high-current bunched mode with a beam-defining aperture of 700 µm. For depth profiling, the machine was operated in a non-interlaced mode in combination with a 5 keV Ar_{2000}^{+} sputter beam (I = 1.328 nA). Low energetic electrons were used for charge compensation during the pause time of 1 s. An analysis area of 70×70 $µm^2$ (128×128 pixels) was chosen in the centre of the 200×200 $µm^2$ sputter area. Depth profiling was stopped at the interface between coating and substrate. Before and after the measurement a scanning probe microscopy image of the analysis area was recorded in intermitted mode with 2048×128 pixels resolution as well as line scans in x and y directions with a scan length of 600 µm each. Data evaluation was carried out with Surface Lab software version 7.3 (IONTOF Company). Negative mass spectra were recorded and the achieved mass resolution was m/Dm >7.500 (FWHM) at m/z = 65.04 ($C_5H_5^-$).

X-Ray Photoelectron Spectroscopy (XPS): XPS measurements were performed using a KRATOS AXIS Ultra DLD (Kratos Analytical, Manchester, United Kingdom) equipped with a monochromatic Al K_α anode working at 15 kV (225 W). For the survey spectra, a pass energy of 160 eV was used while for the region spectra, the pass energy was 20 eV. The investigated area was 700×300 $µm^2$. For all of the PE samples, charge neutralization was necessary. The evaluation and validation of the data were carried out with the software CASA-XPS version 2.3.24. The spectra were calibrated by adjusting the C1s signal to 284.5 eV. For deconvolution of the region files, background subtraction (U 2 Tougaard or Shirley) was performed before calculation.

Electron Paramagnetic Resonance (EPR) Spectroscopy: EPR spectroscopy was performed on a Magnettech Miniscope MS400 X-band benchtop spectrometer (9.30–9.55 GHz). The samples were measured in 4 mm quartz glass EPR tubes at RT and 77K. 5,5-Dimethyl-1-pyrrolin-*N*-oxide (DMPO, 100 mm in either MeOH or benzene) was used as a spin trap to detect short-living radicals. Data evaluation was performed using "ESR-MPlot & Analyze" software. The final examination of recorded EPR spectra was carried out using OriginPro 9.0 software.

DPPH-Radical Detection Assay: The assay was performed according to a modified literature procedure.[49] A 2,2-diphenyl-1-pikryl-hydrazyl (DPPH, 10^{-4} m) stock solution in MeOH and benzene was prepared. A volume of 2 mL DPPH stock solution was added to each test sample. Reactions were carried out for 2 and 24 h at 37 °C (and 70 °C) without stirring. For determination of remaining DPPH-radical, absorptions (A_{520nm}) of sample solutions and DPPH* stock solution were measured via UV/vis spectroscopy at 520 nm. Background absorption of the pure solvent was subtracted. The concentration of remaining DPPH-radical after sample exposition was determined according to Equation 1:

$$\text{Remaining}\,[\text{DPPH}^*]\,(\%) = \frac{A_{520nm}\,(\text{sample}) - A_{520nm}\,(\text{solvent})}{A_{520nm}\,(\text{DPPH stock}) - A_{520nm}\,(\text{solvent})} \times 100 \quad (1)$$

Horseradish Peroxidase (HRP) Assay for Hydrogen Peroxide Detection: Horseradish-peroxidase (0.2 mg mL^{-1}) and pyrogallol (2.5 mg mL^{-1}) were dissolved in a PBS solution (pH adjusted to 8.0). Grafted-poly-*N*-oxide samples were added and incubated for 5 min at 25 °C under gentle shaking. For validation, a positive control with added hydrogen peroxide (0.1 mm) and a negative control without hydrogen peroxide were evaluated under the same conditions. Absorptions (A_{420nm}) of test samples were measured via UV/vis spectroscopy at 420 nm. A blank value of PBS solution was subtracted. Residual enzymatic activity was determined relatively to the H_2O_2-containing positive control using equation 2:

$$\text{Relative HRP activity}\,(\%) = \frac{A_{420nm}\,(\text{sample}) - A_{420nm}\,(\text{solvent})}{A_{420nm}\,(\text{positive control}) - A_{420nm}\,(\text{solvent})} \times 100 \quad (2)$$

Determination of Antibacterial Activity (ASTM E2149-13a): A modified ASTM assay E2149-13a was performed for evaluation of antimicrobial activity. All test samples were sterilized with iPrOH/water mixture (90 vol %)

and subsequently dried under laminar airflow (LAF) prior to testing. The bacterial strains *Staphylococcus aureus* (strain ATCC 29213) and *Escherichia coli* (strain ATCC 25922) were cultured on Columbia agar overnight. The overnight culture was suspended and diluted in sterile saline solution (0.9 %) to preserve a cell density of 1.5×10^8 (OD = 0.5) and diluted to a final concentration of 10^5 colony-forming units per milliliter (CFU mL^{-1}). Zwitterionized and pristine PE test specimens (surface area: 1,0 cm^2) were placed in a 24-well plate (one specimen per well) and covered with 2.0 mL of the respective bacterial suspension (10^5 CFU mL^{-1}). The incubation was carried out at 37 °C under air for 2 h. Afterwards, the incubated solutions and three subsequent dilutions were incubated on Columbia Agar (100 µL of 10^5, 10^4, 10^3 and 10^2 CFU mL^{-1}) for 17 h at 37 °C, prior to cell counting. Colony counts above 250 CFU were set as "too numerous to count" (TNTC). Each experiment was performed as a triplicate. The log10 reduction for each assay was calculated using following equation 3:

$$\log 10 \text{ reduction} = \log\left(\frac{\text{colony forming units (CFU) before exposure}}{\text{colony forming units (CFU) after exposure}}\right) \quad (3)$$

Determination of Low-Fouling Activity (Adhesion Test): All test samples were treated with 90-vol % iPrOH and dried under laminar airflow (LAF) before testing. The strain *Staphylococcus aureus* (strain ATCC 29213) was cultured on Columbia agar overnight. The overnight culture was suspended and diluted in sterile saline solution (0.9 %) to preserve a cell density of 10^4 colony-forming units per milliliter (CFU mL^{-1}). Zwitterionized and pristine PE test specimens (surface area: 1.0 cm^2) were placed in a 24-well plate (one specimen per well) and covered with each 1980 µL of Mueller Hinton Broth (MHB). 20 µL of the bacterial suspension was added to each well to obtain a starting cell density of 10^2 CFU mL^{-1}. The samples were incubated in bacterial solution for 24 h at 37 °C and were subsequently transferred into 3 mL of sterile saline solution without stirring or shaking for 10 min to remove loosely attached bacteria. Each foil was slightly pressed with the modified side onto an agar plate (Columbia agar) and removed after 30 s. Transferred cells were incubated for 20 h at 37 °C prior to cell counting. An aliquot of 100 µL supernatant was taken from each incubation experiment and analyzed with respect to bacterial growth in comparison to a positive control of MHB containing the initial bacterial suspension without added test specimens.

LIVE/DEAD Staining and Confocal Microscopy: Modified poly-*N*-oxide-PE and pristine PE specimens with a surface area of 0.8 cm^2 were immersed in a 6 well plate into 4 mL of *Vibrio campbellii* (strain BB120, OD600nm 0.05) in artificial seawater. The samples were incubated 24 h at 28 °C under gentle shaking (100 rpm) to simulate natural growth conditions. After 24 h test specimens were rinsed with PBS buffer shortly to detach loosely attached planktonic cells. Fluorescence imaging to examine biofilm formation on the test samples was carried out using the LIVE/DEAD *Bac*Light Viability Kit. Images were visualized via confocal laser scanning microscope LSM 800 with AiryScan from Zeiss (Jena, Germany) and edited with ZEN 2 (Blue Edition) software.

Agar Diffusion Plate Test: DIN EN ISO 20645: Leaching of antibacterial components from the poly-*N*-oxide-specimens was evaluated following DIN EN ISO 20645:2002-02 (agar-diffusion assay). Briefly, test specimens were placed with the poly-*N*-oxide-grafted surface facing downwards in a two-layer agar plate (Columbia agar). The top agar layer was previously covered with 200 µL of 1.5×10^8 CFU mL^{-1} of either *S. aureus* (strain ATCC29213) or *E. coli* (strain ATCC25922) suspension. Plates were incubated for 20 h at 37 °C. The plates were then assessed for the development of an inhibition zone surrounding the test specimen.

Determination of Minimum Inhibitory Concentration (MIC): The minimum inhibitory concentration (MIC) of VBNOx, MANOx and MAANOx against *S. aureus* (strain ATCC29213) and *E. coli* (strain ATCC25922) was determined by the microdilution method (Methods for Dilution Antimicrobial Susceptibility Tests for Bacteria That Grow Aerobically; Approved Standard—Ninth Edition. CLSI document M07-A9. Wayne, PA: Clinical and Laboratory Standards Institute; 2012) and compared to the MICs of (vinyl benzyl-)-trimethylammonium chloride (VBTAC) and benzalkonium-chloride (BAC). Tests were performed under air at 37 °C for 20 h. The MIC was defined as the minimum concentration to achieve transparent solutions in the wells. As an upper limit, a concentration of 1024 µg mL^{-1} of the test compounds was used.

Zwitterionization of PE-Foils with Grafted Poly-N-Oxides: PE foils with a thickness of 0.75 mm were rinsed with an isopropanol/water mixture of 70% (v/v) and dried for 15 min at 50 °C prior to use. Plasma treatment of the PE foils was performed at a distance of 6 mm between the plasma jet nozzle and the surface. The speed of the plasma jet nozzle was set at 110 mm s^{-1}. Samples were stored at room temperature under air for 8 min after plasma treatment. In a typical experiment, a solution of the appropriate polymerizable tertiary amine (VBDMA, MADMA or MAADMA) (20 or 40 wt%) and 2,2′-Azobis(isobutyronitrile) (AIBN) as a free radical initiator (0.1 wt% or 1.0 wt%) in EtOAc was purged with nitrogen for 10 min. Plasma-treated PE foils were placed in the degassed solution containing the appropriate polymerizable tertiary amine and AIBN. The resulting reaction mixtures were purged with nitrogen for another 15 min and were subsequently polymerized for 2 h at 85 °C. After polymerization, the materials were treated with a EtOH/water mixture (70vol%) for 15 min with ultrasonication three times and dried for 30 min at room temperature. The resulting specimens were subsequently treated with an aqueous solution of hydrogen peroxide (30% w/w) for 72 h at room temperature under rapid shaking (150 rpm). Residual hydrogen peroxide was destroyed by immersion of the specimens into NaOH solution (1.0 mol L^{-1}) for 24 h at room temperature under gentle shaking. The resulting specimens were washed three times with EtOH/water mixture (70vol%) for each 15 min in an ultrasonic bath and dried for 30 min in a nitrogen stream and were stored before use at room temperature under nitrogen atmosphere.

Statistical Analysis: Statistics were performed using OriginPro 9 (2021) software. Data are reported as mean value ± standard deviation for continuous variables, or as a selective frequency for categorical variables, unless otherwise described. A pairwise comparison with the Tukey test was performed to determine statistical significance. A *p*-value of less than 0.05 (*) was considered significant.

Supporting Information

Supporting Information is available from the Wiley Online Library or from the author.

Acknowledgements

This work was supported by the University of Hamburg.
Open access funding enabled and organized by Projekt DEAL.

Conflict of Interest

The authors declare no conflict of interest.

Data Availability Statement

The data that support the findings of this study are available in the supplementary material of this article.

Keywords

antibacterial materials, antifouling, *N*-oxides, reactive oxygen species, zwitterions

Received: June 15, 2023
Revised: July 25, 2023
Published online:

[1] L. Hall-Stoodley, J. W. Costerton, P. Stoodley, *Nat. Rev. Microbiol.* **2004**, *2*, 95.
[2] Y. X. Wang, J. L. Robertson, W. B. Spillman, R. O. Claus, *Pharm. Res.* **2004**, *21*, 1362.
[3] H. C. Flemming, J. Wingender, U. Szewzyk, P. Steinberg, S. A. Rice, S. Kjelleberg, *Nat. Rev. Microbiol.* **2016**, *14*, 563.
[4] a) S. Galie, C. Garcia-Gutierrez, E. M. Miguelez, C. J. Villar, F. Lombo, *Front. Microbiol.* **2018**, *9*, 898; b) S. L. Percival, L. Suleman, C. Vuotto, G. Donelli, *J. Med. Microbiol.* **2015**, *64*, 323; c) W. Zhou, W. Li, J. Chen, Y. Zhou, Z. Wei, L. Gong, *RSC Adv.* **2021**, *11*, 25484.
[5] a) I. Banerjee, R. C. Pangule, R. S. Kane, *Adv. Mater.* **2011**, *23*, 690; b) D. Rana, T. Matsuura, *Chem. Rev.* **2010**, *110*, 2448; c) A. M. C. Maan, A. H. Hofman, W. M. Vos, M. Kamperman, *Adv. Funct. Mater.* **2020**, *30*, 2000936; d) S. Zheng, M. Bawazir, A. Dhall, H. E. Kim, L. He, J. Heo, G. Hwang, *Front Bioeng Biotechnol* **2021**, *9*, 643722.
[6] M.-C. Sin, S.-H. Chen, Y. Chang, *Polym. J.* **2014**, *46*, 436.
[7] a) A. Venault, Y. Chang, *Langmuir* **2019**, *35*, 1714; b) J. B. Schlenoff, *Langmuir* **2014**, *30*, 9625; c) Y. Chang, *J. Polym. Res.* **2022**, *29*, 286; d) Q. Li, C. Wen, J. Yang, X. Zhou, Y. Zhu, J. Zheng, G. Cheng, J. Bai, T. Xu, J. Ji, S. Jiang, L. Zhang, P. Zhang, *Chem. Rev.* **2022**, *122*, 17073; e) S. Paschke, K. Lienkamp, *ACS Applied Polymer Materials* **2020**, *2*, 129.
[8] Q. Shao, S. Jiang, *J. Phys. Chem. B* **2014**, *118*, 7630.
[9] R. G. Chapman, E. Ostuni, S. Takayama, R. E. Holmlin, L. Yan, G. M. Whitesides, *J. Am. Chem. Soc.* **2000**, *122*, 8303.
[10] a) S. Hiranphinyophat, Y. Iwasaki, *Sci. Technol. Adv. Mater.* **2021**, *22*, 301; b) K. Ishihara, N. P. Ziats, B. P. Tierney, N. Nakabayashi, J. M. Anderson, *J. Biomed. Mater. Res.* **1991**, *25*, 1397.
[11] B. Cao, Q. Tang, G. Cheng, *J. Biomater. Sci., Polym. Ed.* **2014**, *25*, 1502.
[12] a) A. B. Lowe, M. Vamvakaki, M. A. Wassall, L. Wong, N. C. Billingham, S. P. Armes, A. W. Lloyd, *J Biomed Mater Res* **2000**, *52*, 88; b) C. Viklund, K. Irgum, *Macromolecules* **2000**, *33*, 2539; c) Y. Zhang, Y. Liu, B. Ren, D. Zhang, S. Xie, Y. Chang, J. Yang, J. Wu, L. Xu, J. Zheng, *J. Phys. D: Appl. Phys.* **2019**, *52*, 403001.
[13] a) Q. Shao, S. Jiang, *J. Phys. Chem. B* **2013**, *117*, 1357; b) H. Du, X. Qian, *J. Comput. Chem.* **2016**, *37*, 877; c) C. Y. Chiu, Y. Chang, T. H. Liu, Y. N. Chou, T. J. Yen, *J. Mater. Chem. B* **2021**, *9*, 8437; d) S. Abraham, A. So, L. D. Unsworth, *Biomacromolecules* **2011**, *12*, 3567; e) Y. Higaki, J. Nishida, A. Takenaka, R. Yoshimatsu, M. Kobayashi, A. Takahara, *Polym. J.* **2015**, *47*, 811; f) J. F. Karthäuser, J. Koc, E. Schönemann, R. Wanka, N. Aldred, A. S. Clare, A. Rosenhahn, A. Laschewsky, *Advanced Materials Interfaces* **2022**, *9*, 2200677.
[14] B. Li, P. Jain, J. Ma, J. K. Smith, Z. Yuan, H. C. Hung, Y. He, X. Lin, K. Wu, J. Pfaendtner, S. Jiang, *Sci. Adv.* **2019**, *5*, 9562.
[15] I. O'Neil, *Sci. Synth.* **2009**, *40*, 860.
[16] E. P. Linton, *J. Am. Chem. Soc.* **1940**, *62*, 1945.
[17] J. Hunger, N. Ottosson, K. Mazur, M. Bonn, H. J. Bakker, *Phys. Chem. Chem. Phys.* **2015**, *17*, 298.
[18] Q. Zou, B. J. Bennion, V. Daggett, K. P. Murphy, *J. Am. Chem. Soc.* **2002**, *124*, 1192.
[19] Q. Zhang, M. A. Kelland, H. Frey, J. Blankenburg, L. Limmer, *Energy Fuels* **2020**, *34*, 6298.
[20] J. Zhen, Z. Zhou, M. He, H. X. Han, E. H. Lv, P. B. Wen, X. Liu, Y. T. Wang, X. C. Cai, J. Q. Tian, M. Y. Zhang, L. Xiao, X. X. Kang, *Front. Endocrinol. (Lausanne)* **2023**, *14*, 1085041.
[21] a) A. Rani, A. Jayaraj, B. Jayaram, V. Pannuru, *Sci. Rep.* **2016**, *6*, 23656; b) Y. T. Liao, A. C. Manson, M. R. DeLyser, W. G. Noid, P. S. Cremer, *Proc. Natl. Acad. Sci. USA* **2017**, *114*, 2479; c) T. C. Gluick, S. Yadav, *J. Am. Chem. Soc.* **2003**, *125*, 4418.
[22] a) R. Lindigkeit, A. Biller, M. Buch, H. M. Schiebel, M. Boppre, T. Hartmann, *Eur. J. Biochem.* **1997**, *245*, 626; b) T. Hartmann, G. Toppel, *Phytochemistry* **1987**, *26*, 1639; c) V. M. Dembitsky, T. A. Gloriozova, V. V. Poroikov, *Phytomedicine* **2015**, *22*, 183.
[23] R. D. Bach, H. B. Schlegel, *J. Phys. Chem. A* **2021**, *125*, 5014.
[24] a) D. Bernier, U. K. Wefelscheid, S. Woodward, *Org. Prep. Proced. Int.* **2009**, *41*, 173; b) A. Petrosyan, R. Hauptmann, J. Pospech, *Eur. J. Org. Chem.* **2018**, *2018*, 5237; c) A. M. Bauer, E. E. Ramey, K. G. Oberle, G. A. Fata, C. D. Hutchison, C. R. Turlington, *Tetrahedron Lett.* **2019**, *60*, 151193.
[25] D. Yan, K. Wang, S. Bai, B. Liu, J. Bai, X. Qi, Y. Hu, *J. Am. Chem. Soc.* **2022**, *144*, 4269.
[26] a) G. Cheng, B. Li, C. Wang, H. Zhang, G. Liang, Z. Weng, H. Hao, X. Wang, Z. Liu, M. Dai, Y. Wang, Z. Yuan, *PLoS One* **2015**, *10*, 0136450; b) Z. Shah, R. Mahbuba, B. Turcotte, *FEMS Microbiol. Lett.* **2013**, *347*, 61; c) C. Avendaño, J. C. Menéndez, in *Medicinal Chemistry of Anticancer Drugs*, (Eds.: C. Avendaño, J. C. Menéndez), Elsevier, Amsterdam **2008**, p. 93; d) S. E. Walsh, J. Y. Maillard, A. D. Russell, C. E. Catrenich, D. L. Charbonneau, R. G. Bartolo, *J. Appl. Microbiol.* **2003**, *94*, 240; e) P. Wardman, K. I. Priyadarsini, M. F. Dennis, S. A. Everett, M. A. Naylor, K. B. Patel, I. J. Stratford, M. R. L. Stratford, M. Tracy, *Br. J. Cancer* **1996**, *74*, 70.
[27] X. Shen, K. S. Gates, *Chem. Res. Toxicol.* **2019**, *32*, 348.
[28] a) M. Lv, Y. Li, X. Wei, Y. Xu, Z. Ge, X. Chen, *ACS Appl. Energy Mater.* **2019**, *2*, 2238; b) A. C. Griffin, A. M. Bhatti, G. A. Howell, *MRS Online Proc. Libr.* **1987**, *109*, 115.
[29] a) H. W. Schlipköter, A. Brockhaus, *Klin. Wochenschr.* **1961**, *39*, 1182; b) N. G. Puchkova, A. V. Nekrasov, Y. F. Razvodovskii, B. S. El'tsefon, *Polymer Science U.S.S.R* **1980**, *22*, 1407.
[30] N. Zhang, K. Cheng, J. Zhang, N. Li, X. Yang, Z. Wang, *J. Membr. Sci.* **2022**, *660*, 120829.
[31] a) S. Kliewer, S. G. Wicha, A. Broker, T. Naundorf, T. Catmadim, E. K. Oellingrath, M. Rohnke, W. R. Streit, C. Vollstedt, H. Kipphardt, W. Maison, *Colloids Surf., B* **2020**, *186*, 110679; b) N. Burmeister, C. Vollstedt, C. Kröger, T. Friedrich, N. Scharnagl, M. Rohnke, E. Zorn, S. G. Wicha, W. R. Streit, W. Maison, *Colloids Surf., B* **2023**, *224*, 113195.
[32] F. Khalil, E. Franzmann, J. Ramcke, O. Dakischew, K. S. Lips, A. Reinhardt, P. Heisig, W. Maison, *Colloids Surf., B* **2014**, *117*, 185.
[33] G. L. Archer, *Clin. Infect. Dis.* **1998**, *26*, 1179.
[34] a) I. Karunasagar, S. K. Otta, I. Karunasagar, *Aquaculture* **1996**, *140*, 241; b) C. M. Waters, B. L. Bassler, *Genes Dev.* **2006**, *20*, 2754.
[35] S. Guo, D. Jańczewski, X. Zhu, R. Quintana, T. He, K. G. Neoh, *J. Colloid Interface Sci.* **2015**, *452*, 43.
[36] C. Zhang, J. Zhou, X. Ye, Z. Li, Y. Wang, *Macromolecules* **2021**, *54*, 4236.
[37] M. van de Lagemaat, A. Grotenhuis, B. van de Belt-Gritter, S. Roest, T. J. A. Loontjens, H. J. Busscher, H. C. van der Mei, Y. Ren, *Acta Biomater.* **2017**, *59*, 139.
[38] H.-C. Flemming, J. Wingender, *Nat. Rev. Microbiol.* **2010**, *8*, 623.
[39] Z. Temoçin, M. Yiğitoğlu, *Bioprocess Biosyst. Eng.* **2009**, *32*, 467.
[40] Y. S. Raval, L. Flurin, A. Mohamed, K. E. Greenwood-Quaintance, H. Beyenal, R. Patel, *Antimicrob. Agents Chemother.* **2021**, *65*, 01966.
[41] O. P. Sharma, T. K. Bhat, *Food Chem.* **2009**, *113*, 1202.
[42] J. P. Gotham, R. Li, T. E. Tipple, J. R. Lancaster, T. Liu, Q. Li, *Free Radical Biology and Medicine* **2020**, *154*, 84.
[43] a) L. Zhang, J. Sun, W. Huang, S. Zhang, X. Deng, W. Gao, *J. Am. Chem. Soc.* **2023**, *145*, 1707; b) J. Jin, P. Yuan, W. Yu, J. Lin, A. Xu, X. Xu, J. Lou, T. Yu, C. Qian, B. Liu, J. Song, L. Li, Y. Piao, T. Xie, Y. Shen, H. Tao, J. Tang, *ACS Nano* **2022**, *16*, 10327; c) H. Zhang, C.-H. Huang, *Environ. Sci. Technol.* **2005**, *39*, 593.
[44] H. Huang, C. Zhang, R. Crisci, T. Lu, H. C. Hung, M. S. J. Sajib, P. Sarker, J. Ma, T. Wei, S. Jiang, Z. Chen, *J. Am. Chem. Soc.* **2021**, *143*, 16786.

[45] W. Fan, Q. Wei, J. Xiang, Y. Tang, Q. Zhou, Y. Geng, Y. Liu, R. Sun, L. Xu, G. Wang, Y. Piao, S. Shao, Z. Zhou, J. Tang, T. Xie, Z. Li, Y. Shen, *Adv. Mater.* **2022**, *34*, 2109189.
[46] X. Guan, K. Zhang, F. Huang, G. C. Bazan, Y. Cao, *Adv. Funct. Mater.* **2012**, *22*, 2846.
[47] A. L. J. Beckwith, P. H. Eichinger, B. A. Mooney, R. H. Prager, *Aust. J. Chem.* **1983**, *36*, 719.
[48] P. F. Holt, *Br. J. Ind. Med.* **1971**, *28*, 72.
[49] M. Suzuki, A. Kishida, H. Iwata, Y. Ikada, *Macromolecules* **1986**, *19*, 1804.